J Mater Sci (2019) 54:14038–14054

Computation & theory

Vibration reduction design method of metamaterials with negative Poisson's ratio

Haoxing Qin[1] and Deqing Yang[1,*]

[1] *Collaborative Innovation Center for Advanced Ship and Deep-Sea Exploration, State Key Laboratory of Ocean Engineering, School of Naval Architecture, Ocean and Civil Engineering, Shanghai Jiao Tong University, Shanghai 200240, China*

Received: 11 April 2019
Accepted: 1 August 2019
Published online: 16 August 2019

ABSTRACT

This work proposes a topology optimization design method of metamaterials for improving the vibration reduction performance. Firstly, an optimization mathematical model of the functional element is established with the objective of maximizing the origin mechanical impedance level, and the functional element with optimal vibration reduction effect is obtained by the calculation of the mathematical model. Then, the optimized functional elements are periodically arranged to generate the metamaterials, and thus a series of metamaterials with negative Poisson's ratio ranging from − 0.5 to − 2.0 are designed. Numerical simulation shows that the amplitudes of the acceleration response are reduced by 66.5% after the vibration is passed through the metamaterials. Comparison shows that the novel designed metamaterials achieve at least 12% improvement in vibration reduction performance over the traditional honeycomb.

Introduction

The material with positive Poisson's ratio (PR) exhibits a phenomenon of swelling in a direction perpendicular to the direction of compression. Conversely, the material with negative PR exhibits shrink in the transverse direction when compressed [1, 2]. Compared with traditional positive PR materials [3, 4], negative PR metamaterials exhibit superior mechanical properties and application prospects [5] in terms of indentation resistance [6], lightweight [7], impact resistance [8, 9], energy absorption [10, 11] and vibration reduction [12, 13].

In terms of dynamics, negative PR metamaterials show superiority over traditional materials in reducing vibration propagation [14, 15]. Duc et al. [16, 17] investigated the nonlinear dynamic response and vibration of composite double-curved shallow shells with auxetic cellular, and the effects of material properties, geometrical parameters, elastic foundations, auxetic core layer and blast loads on nonlinear dynamic response were analyzed to guide the design of auxetic composite structure. Reviews in [18] presented the advantages of negative PR metamaterials in damping and acoustics. Scarpa et al. [19] studied the transmission of vibration waves in conventional materials and negative PR metamaterials and concluded that metamaterials with negative PR show better vibration reduction performance for wave propagation. In addition, the conclusions from

Address correspondence to E-mail: yangdq@sjtu.edu.cn

https://doi.org/10.1007/s10853-019-03903-z

numerical simulations and experiments are used to guide the prediction and design of acoustic properties of negative PR metamaterials [20, 21]. Unlike traditional periodic auxetic materials, when the functionally graded materials are subjected to vibration or shock, the dynamic response and deformation of the local structure change with the change of the cell gradient, which can reduce the local stress concentration to ensure the integrity and reliability of the structure [22, 23]. Ajdari et al. [24] studied the mechanical properties of density gradient honeycomb structures under uniaxial and biaxial plane impact using finite element and theoretical methods. Previous studies on dynamics and vibration response have focused more on examining mechanics, properties and applications through simulations and experimental tests [18]. As mentioned in the work by [25], how to design a metamaterial structure with specified properties is more practical.

The design of the mechanical properties has received great attention in mitigating vibration. It is revealed in [26] that the formation of the band gap can be traced back to the resonant behavior of the elementary building blocks of the honeycomb structure under different boundary conditions and concluded that the damping band gap can be designed to achieve the purpose of vibration reduction. Afterward, optimization design is recognized as an effective way to improve mechanical properties, where the size and shape optimizations are two common optimization methods with features of being convenient and effective. For the applications of size or shape optimizations [27], metamaterials are designed by optimizing the cell wall thickness, cell angle, cell height and cell length [28–30]. The above improved methods based on the conventional configuration are insufficient for improving the mechanical properties of metamaterials [31, 32]. Moreover, the unique performance of metamaterials is strongly dependent on the configurations of the underlying substructure; that is to say, many interesting properties of metamaterials can be obtained through innovative configuration design of metamaterials' substructure [33, 34].

The reviews on metamaterials topology optimization for dynamics are concluded in [35, 36]. Previous work by [37] proposed a functional element topology optimization (FETO) method, which optimizes the configuration of substructures and then periodically arranges the substructures to generate metamaterials. Consequently, this work proposed a FETO-based vibration reduction design method; then, a series of novel configurations metamaterials with specified negative PR are designed to improve the vibration reduction performance.

This work is organized as follows. In ''Metamaterials design for vibration reduction'' section, the FETO-based vibration reduction design method is described in detail, and the concept of mechanical impedance is introduced to evaluate the vibration reduction effect. In "Formulation of the optimization problem'' section, a mathematical model is established to perform the configuration design of metamaterials. "Numerical simulation of the metamaterials" section analyzes the dynamic properties of metamaterials and summarizes the effect of PR to the vibration reduction performance. In "Evaluation of vibration reduction performance" section, comparison of the vibration reduction of novel metamaterials and honeycomb is performed.

Metamaterials design for vibration reduction

Based on the FETO method, a design method of metamaterials with vibration reduction performance is proposed in this section and the concept of mechanical impedance is introduced to evaluate the vibration reduction effect.

Definition of functional elements and metamaterials

Figure 1 illustrates the main idea of the FETO method. The initial materials structure to be designed is subdivided into several design domains, and the single design domain is discretized into finite element meshes; that is, the functional element topology optimization design of this work is carried out in the design area.

Mechanical impedance to evaluate vibration reduction

Generally, the vibration reduction effect can be expressed as the ratio of the vibration response at the excitation location to the response at the output location; the greater the ratio, the better the vibration reduction effect. Since the distribution path of

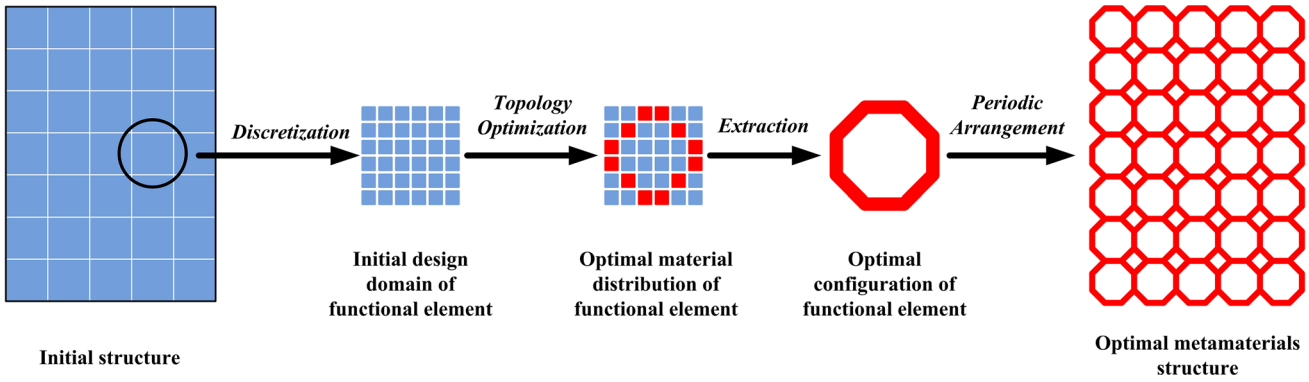

Figure 1 Schematic of design method of metamaterials based on functional element topology optimization.

materials is uncertain during the optimization calculation iteration, it is not conducive to collecting the input and output responses of all finite element nodes. Once the mechanical impedance is used to describe the vibration reduction effect, it is only necessary to collect the response of the excitation position without obtaining a response to the output position. This is due to the fact that the mechanical impedance of the excitation position is an inherent feature of structural vibration and can reflect the vibration reduction effect of the metamaterials and structures.

Definition of mechanical impedance

Mechanical impedance is a key indicator of structural dynamic characteristic, which directly reflects the structural dynamic performance under external excitation [38, 39], and the generalized mechanical impedance is defined as the ratio of harmonic excitation force to the response caused by it. It is well known that the vibration response can be represented in terms of displacement, velocity and acceleration. Similarly, the mechanical impedance can also be classified into displacement impedance, velocity impedance and acceleration impedance.

In this work, the acceleration impedance is used to describe the mechanical impedance of metamaterials:

$$Z = \frac{F_i}{X_j} \tag{1}$$

where F_i is the input excitation force acting on node i and X_j is the output acceleration response of node j.

Conversion between the mechanical impedance and vibration reduction

Figure 2 shows the definition of mechanical impedance in functional element. For a forced vibration system, the input acceleration response at the excitation position is denoted as a_0, and the output acceleration response after the vibration transmission is denoted as a_n. The transmission rate (T_a) and vibration level difference (VLD) can be expressed as:

$$T_a = \frac{a_n}{a_0} \tag{2}$$

$$\mathrm{VLD} = 20\log_{10}\left(\frac{a_0}{a_n}\right) = 20\log_{10}\left(\frac{a_0/a_{ref}}{a_n/a_{ref}}\right) = L_1 - L_2 \tag{3}$$

where L_1 is the input acceleration level at the excitation position, L_2 is the output acceleration level at the response position and a_{ref} is the reference value of acceleration.

The relationship between VLD and T_a is

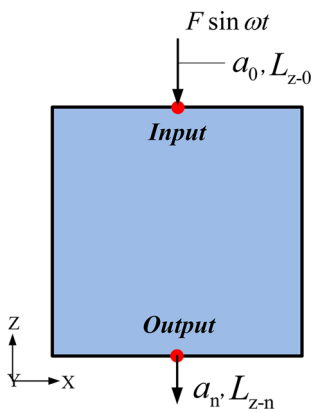

Figure 2 Definition of the mechanical impedance in functional element.

$$\mathrm{VLD} = 20\log_{10}\left(\frac{a_0}{a_n}\right) = 20\log_{10}\frac{1}{T_a}, \tag{4}$$

and the relationship between impedance and T_a can be expressed as

$$T_a = \frac{a_n/F}{a_0/F} = \frac{Z_0}{Z_n} \tag{5}$$

where Z_0 represents the origin impedance at the excitation position and Z_n represents the impedance at the response position.

Similar to the definition of the VLD in Eq. (3), this work defines an impedance level L_z to characterize the structural vibration transmission properties

$$L_z = 20\log_{10}\frac{Z}{Z_{ref}} \tag{6}$$

where Z_{ref} represents the reference value of impedance, and this work takes $Z_{ref} = 1\,\mathrm{Ns^2/m}$.

Substituting Eq. (5) into Eq. (4) yields

$$\mathrm{VLD} = 20\log_{10}\frac{Z_n}{Z_0} = 20\log_{10}\left(\frac{Z_n/Z_{ref}}{Z_0/Z_{ref}}\right) = L_{zn} - L_{z0} \tag{7}$$

where L_{z0} represents the origin impedance level of the vibration excitation and L_{zn} represents the transmission impedance level after the vibration transmission.

In this work, the difference between impedance levels is defined as the impedance level difference (ILD):

$$\mathrm{ILD} = L_{zn} - L_{z0}. \tag{8}$$

Although the value of VLD in Eq. (7) is equal to the value of ILD in Eq. (8), the physical meaning is quite different. From Eq. (2), when the transmission ratio T_a is constant, the output acceleration response a_n decreases as the input acceleration response a_0 decreases, thereby achieving the purpose of reducing the output vibration response after the vibration propagation of metamaterials. In addition, it can be seen from Eqs. (1) and (6) that the decrease in a_0 leads to an increase in L_{z0}. Therefore, maximizing L_{z0} as an optimization objective can be used to improve the vibration reduction performance of metamaterials.

In order to intuitively reflect the mechanical impedance properties of the structure, a concept of synthesized origin impedance level $\bar{L}_{z0}$ is defined to synthesize the values of impedance level in the sweep frequency range:

$$\bar{L}_{z0} = 10\log_{10}\sum_{i=1}^{S} 10^{0.1L^i_{z0}} \tag{9}$$

where L^i_{z0} is the origin impedance level at a specified frequency f_i and S is the number of the sweep frequency.

Macroscopic effect of Poisson's ratio

The general methods for calculating PR values of a metamaterials can be used for common cell configurations [40–42], but it is not suitable for the PR calculation of cells with irregular shapes in topology optimization process. The following scholars have studied the macro-PR evaluation method to solve the above problems. Previous work by [43, 44] presented a method to study the macroscopic mechanical properties of materials by applying simple loads to characterize the macroscopic mechanical properties of materials under complex stress conditions. Carneiro et al. [45] introduced a PR evaluation method in material mechanics test to analyze the macroscopic PR effect of cellular material.

In this work, the method in [45] is also used to describe the macroscopic PR effect during the optimization iteration of functional element. The cell configuration in Fig. 3 is an example to calculate the macroscopic PR of metamaterial in detail. The strain of the cell configuration is

$$\varepsilon_X = 2\frac{\Delta x_2}{x_2}, \quad \varepsilon_Z = 2\frac{\Delta z_1}{z_1} \tag{10}$$

where ε_X and ε_Z are the strain in X- and Z-directions, Δx_2 and x_2 are the displacement and coordinate position of point n_2 in X-direction and Δz_1 and z_1 are the displacement and coordinate position of point n_1 in Z-direction.

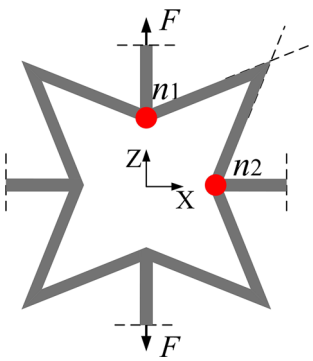

Figure 3 Evaluation method of the macroscopic PR effect.

Then, the PR evaluation of the cell configuration in Fig. 3 can be expressed as:

$$v_{ZX} = -\frac{\varepsilon_X}{\varepsilon_Z}. \tag{11}$$

Formulation of the optimization problem

This section describes the details of a metamaterials design, and Fig. 4 illustrates the optimization design of functional element and the construction of metamaterials. In this work, a series of metamaterials with various PRs are designed to analyze the effect of PR on vibration reduction performance [46, 47] and to verify the reliability of the proposed method of metamaterials vibration reduction design.

Topology optimization calculation in this work is carried out by the commercial software of Hyperworks/OptiStruct. The scheme materials model of the optimization adopts the SIMP method (solid isotropic materials with penalization), and the general idea is to introduce a fictitious density variables field to penalize, for each element, some relevant physical quantities like element stiffness tensor, materials density, etc. The relationships between the relative density and the elastic modulus of materials are as follows:

$$E(x_e) = E_{\min} + x_e^p(E_0 - E_{\min}) \tag{12}$$

$$\mathbf{K} = \sum_{e=1}^{N} \left(E_{\min} + x_e^p \Delta E\right)\mathbf{k}_0 \tag{13}$$

where $x_e(e = 1, 2, \cdots N)$ is the relative density of element e; N is the number of elements; E_0 and $E_{\min}$ are the initial elastic modulus of the elements and the elastic modulus of the hole elements; $\Delta E = E_0 - E_{\min}$, $E_{\min} = E_0/1000$; p is the penalty factor; $E(x_e)$ is the elastic modulus after interpolation; $\mathbf{K}$ is the global stiffness matrix which can be obtained as the sum of elemental stiffness over all N elements; and $\mathbf{k}_0$ is the initial stiffness matrix of each mesh element.

Due to the existence of semi-dense elements, the analysis results may change dramatically when the design process enters a new phase using a different penalization factor. In OptiStruct, the discrete parameter corresponds to penalty factor, and it usually takes a value between 2.0 and 4.0. The default discrete value is 1.0 for shell dominant structures and 2.0 for solids dominant structures. (The dominance is defined by the proportion of number of elements.) When minimum member size control is used, the penalty starts at 2 and is increased to 3 for the second and third iterative phases. For other manufacturing constraints such as draw direction, extrusion, pattern repetition and pattern grouping, the penalty starts at 2 and increases to 3 and 4 for the second and third iterative phases, respectively.

Modeling of optimization problem

As shown in Fig. 5, the design domain is discretized into 84 × 84 finite element meshes, and the type of the elements is plate. Within the frequency range between 10 and 300 Hz, a sinusoidal excitation force

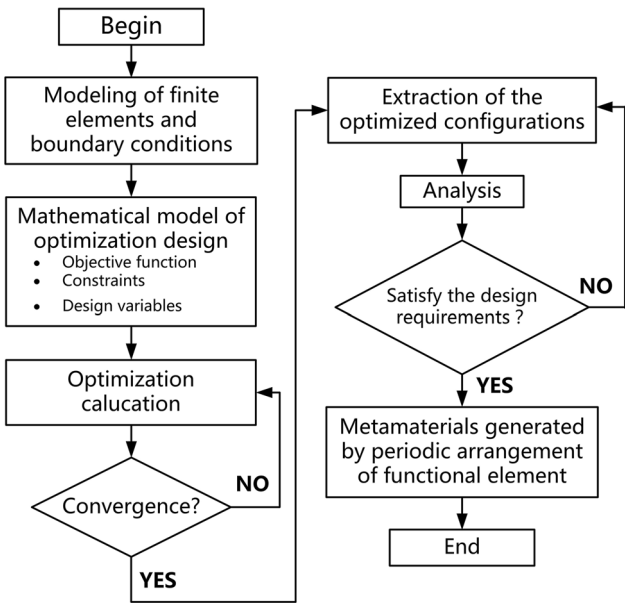

Figure 4 Flowchart of the vibration reduction design method of metamaterials.

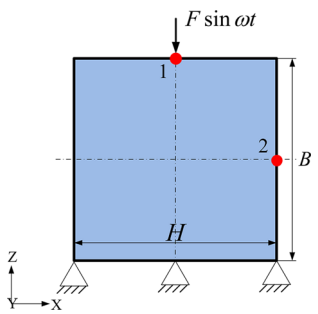

Figure 5 Design domain and loading of the functional element topology optimization ($B = H = 42$ mm).

with an amplitude of $F = 10\,\mathrm{N}$ is applied to the center of the upper faceplate while the lower faceplate is fixed. The measuring points 1 and 2 (in Fig. 5) are used to evaluate the macroscopic Poisson's ratio effects. The metamaterials are made of PLA (polylactic acid) with Young's modulus $E_\mathrm{P} = 2636\,\mathrm{MPa}$, density $\rho_\mathrm{P} = 1180\ \mathrm{kg/m^3}$ and materials Poisson's ratio $v_\mathrm{P} = 0.38$.

From the Poisson's ratio in Eq. (11), we can express the macroscopic Poisson's ratio in Fig. 5 as follows:

$$v = -\frac{\varepsilon_2}{\varepsilon_1} = -\frac{\Delta u_2}{\Delta w_1}\cdot\frac{B}{H} \tag{14}$$

where Δw_1 and Δu_2 represent the displacement of points 1 in Z-direction and the displacement of points 2 in X-direction.

This paragraph describes the mathematical model of vibration reduction optimization design for metamaterials. Regarding the setting of the objective function, the purpose of maximizing the synthetic origin impedance level $\bar{L}_{z0}$ as the objective of vibration reduction is explained in "Mechanical impedance to evaluate vibration reduction" section. In this work, the optimization problem is described as: within a certain specified amount of materials, the PR is set as the constraint, and the maximization of the origin impedance level is taken as the objective. Then, the mathematical model of optimization is

$$\begin{cases} \text{find} & \mathbf{X} = [x_1, x_2, \cdots, x_N]^\mathrm{T} \\ \max & \bar{L}_{z0} \\ \text{s.t.} & \mathbf{M}\ddot{\mathbf{U}} + \mathbf{K}\mathbf{U} = \mathbf{F} \\ & |v - v_0| \le \varepsilon \\ & f'_{\mathrm{vol}} \le V(\mathbf{X})/V_0 \le f''_{\mathrm{vol}} \\ & 0 < x_{\min} \le x_e \le x_{\max} \le 1 \\ & e = 1, \ldots, N \end{cases} \tag{15}$$

where $\mathbf{X} = [x_1, x_2, \cdots, x_N]^\mathrm{T}$ is the vector of design variables. $x_{\max}$ and $x_{\min}$ are the upper and lower limits of design variables, respectively (nonzero to avoid singularity). $\bar{L}_{z0}$ denotes the synthesized origin impedance level. The global stiffness matrix can be obtained as the sum of elemental stiffness over all N elements, i.e., $\mathbf{K} = \sum_{e=1}^{N} x_e^p \mathbf{k}_0$. $\mathbf{M} = \sum_{e=1}^{N} x_e^p \mathbf{m}_0$ is the total mass of the functional element, where $\mathbf{m}_0$ is the initial mass of each mesh element. $\mathbf{U}$ and $\mathbf{F}$ are the global vector of displacements and forces. $\mathbf{u}_e$ is the displacement vector of mesh element. $V(\mathbf{X})$ is the total structural volume in the optimization progress; V_0 is the initial total volume when the relative density of the design domain area is 1. f'_{vol} and f''_{vol} are the lower limit and upper limit volume fraction of the materials in design domain. $|v - v_0| \le \varepsilon$ is the constraint of PR, where v and v_0 represent the PR in the optimization iteration and the PR of the specified design requirements, respectively.

Optimized configurations of functional element

Considering that the amount of material used in the structural topology optimization design has a great influence on the configuration of the optimized functional element, the setting of the volume fraction (f'_{vol} and f''_{vol}) in the optimization model of this work considers the following two aspects: The lower limit f'_{vol} is set to 20% to ensure the stability of the optimized structure, and the upper limit f''_{vol} is set to 30% to avoid the metamaterials being too heavy after optimization.

As shown in Fig. 6, the four functional elements corresponding to PR with $v = -0.5, -1.0, -1.5$ and -2.0 are generated by calculating Eq. (15), and the synthesized origin impedance levels $\bar{L}_{z0}$ [in Eq. (9)] after optimization iteration are 24.6 dB, 29.7 dB, 32.1 dB and 32.8 dB, respectively.

Although the wall thickness of the configuration in Fig. 6 is not uniform, Gibson [41] verified that the wall thickness has a negligible effect on the mechanical properties when the wall thickness is much smaller than the cell size. Therefore, under the premise of ignoring the influence of wall thickness on mechanical properties, the wall thickness of the extracted configurations is designed to be $t = 1\,\mathrm{mm}$, and the uniformly spaced grid is employed herein to represent the irregular configurations of the functional elements (as shown in Fig. 7).

Verification of the PR values of metamaterials

Since the extraction of the optimization results may cause errors, this paragraph reanalyzes the extracted configurations by finite element analysis. The extracted configurations in Fig. 7 are established as the finite element model for static analysis, and the actual PR of extracted configuration in Fig. 7 can be calculated according to Eq. 11; therefore, the error ratio between the actual PR after extraction and the PR of design requirement can be calculated. As shown in Fig. 8 and Fig. 9, the PR error rate analysis

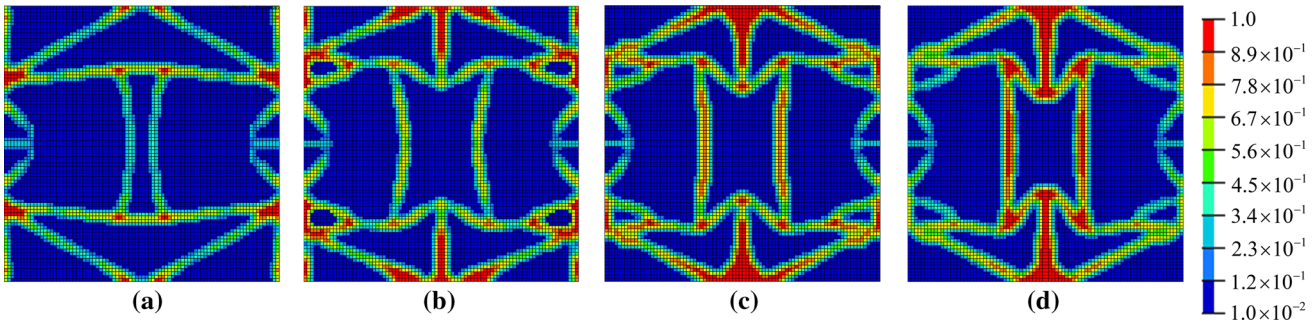

Figure 6 Optimal configurations of the functional element corresponding to various PRs: **a** $v=-0.5$; **b** $v=-1.0$; **c** $v=-1.5$; **d** $v=-2.0$.

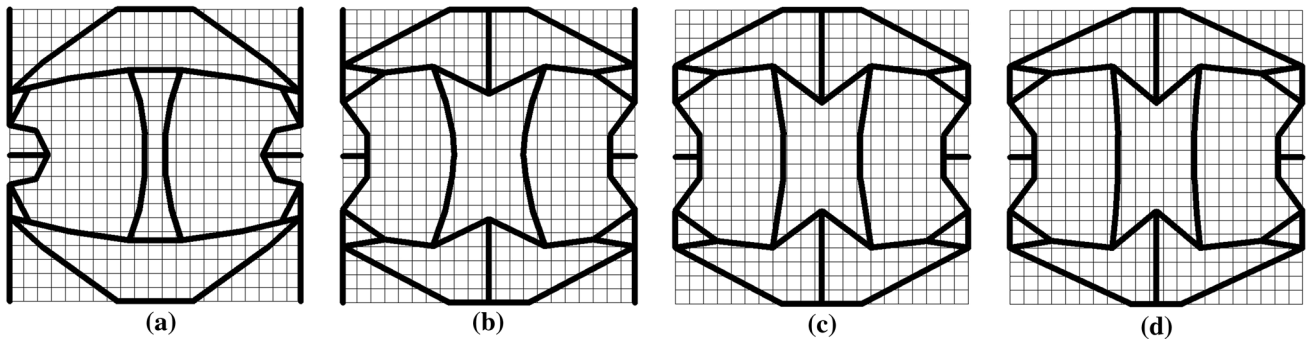

Figure 7 Extraction of the optimal configurations corresponding to various PRs: **a** $v=-0.5$; **b** $v=-1.0$; **c** $v=-1.5$; and **d** $v=-2.0$.

of functional element with $v=-1.5$ is taken as an example to describe the calculation method of the PR error rate in detail. The reanalysis of the extracted configuration is summarized in Table 1, and the comparison shows that the Poisson's ratio before and after the extraction is roughly consistent.

Metamaterials based on periodic arrangement of functional element

As shown in Fig. 6 and Fig. 7, the configurations of the functional elements with maximization vibration reduction performance are designed after optimization. Afterward, the extracted and verified functional elements are periodically arranged into the metamaterials. Figure 10 shows the corresponding functional elements, metamaterials and specimen with $v=-0.5$, wherein the specimen is fabricated by additive manufacturing.

Numerical simulation of the metamaterials

The metamaterials are generated by ordering the functional elements. Each optimal configuration in Fig. 7 is periodically arranged in a cycle of 8×8 to

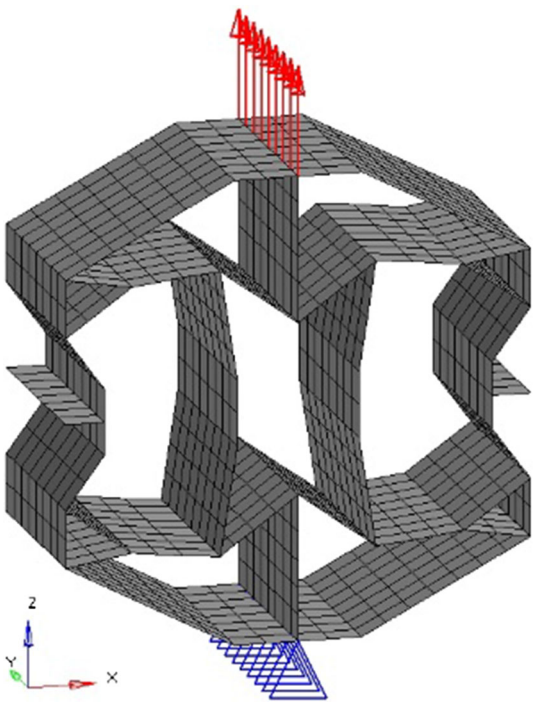

Figure 8 Finite element model of the extracted functional element with $v=-1.5$, which is established according to the dimensions of Fig. 7c.

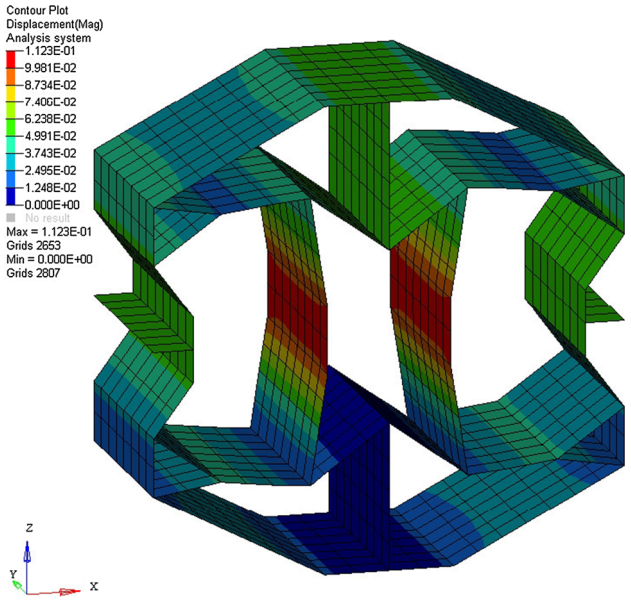

Figure 9 Displacement analysis of the extracted functional element with $v = -1.5$.

form the metamaterials in Fig. 11. Within the frequency range between 10 and 300 Hz, a sinusoidal excitation force with an amplitude of $F = 10$ N is applied to the center of the upper faceplate while the lower faceplate is fixed, where the thicknesses of both faceplates are 10 mm. The outline dimension of each metamaterial is 336 mm × 356 mm, and the depth perpendicular to the page is 20 mm. The metamaterials are made of PLA (polylactic acid) with Young's modulus $E_P = 2636$ MPa, density $\rho_P = 1180$ kg/m^3 and materials Poisson's ratio $v_P = 0.38$.

Next, the dynamic characteristics of each metamaterial in Fig. 11 will be analyzed by the software of Hyperworks. Within the frequency range between 10 and 300 Hz, a sinusoidal excitation force with an amplitude of $F = 10$ N is applied to the center of the upper faceplate while the lower faceplate is fixed, and the critical damping values of the structural vibration analysis in this work are uniformly set as

Table 1 Relative errors of PR between the extracted configurations and design requirements

Design requirements	$v = -0.5$	$v = -1.0$	$v = -1.5$	$v = -2.0$
After extraction	$v' = -0.53$	$v' = -1.085$	$v' = -1.54$	$v' = -2.16$
Relative error ratio (%)	6.0	8.5	2.7	8.0

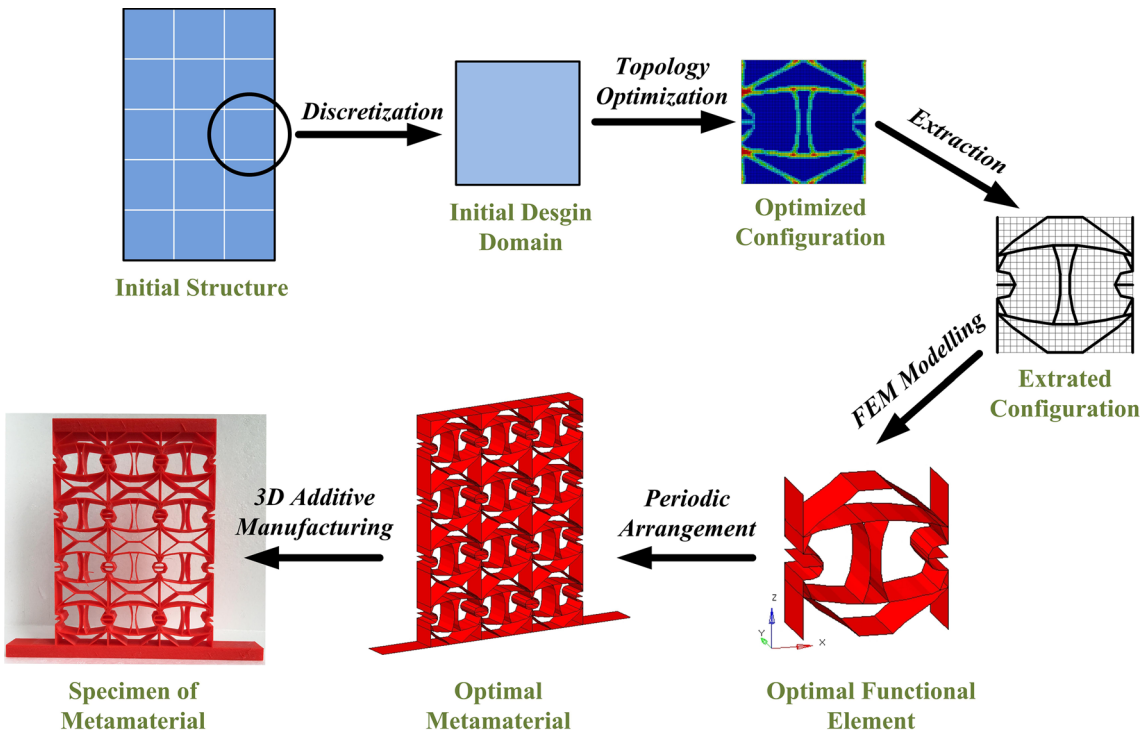

Figure 10 Optimal functional element, metamaterials and 3D-printed specimen, with corresponding PR $v = -0.5$.

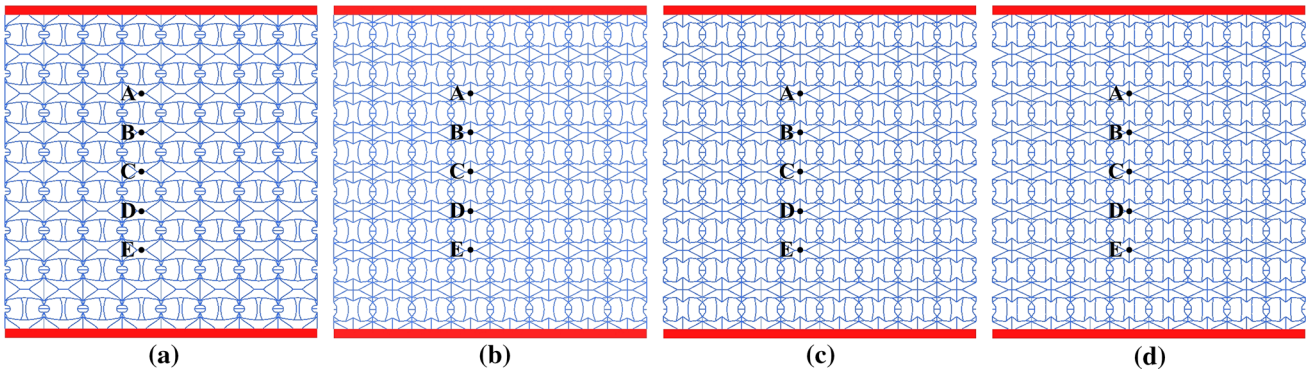

Figure 11 Metamaterials corresponding to various PRs : **a** $v = -0.5$; **b** $v = -1.0$; **c** $v = -1.5$; and **d** $v = -2.0$.

1%. The modal analysis of the vertical first-order natural frequency is summarized in Table 2, and the frequency response analysis calculates the frequency response curves of the measuring points (A, B, C, D and E) in each metamaterial (as shown in Fig. 12).

Vibration reduction performance

The vibration reduction performance of the four metamaterials is described by analyzing the frequency response characteristics of several functional elements at the center of metamaterials, where the frequency response characteristics of each functional element can be represented by the frequency response of the measuring points (a–e in Fig. 11) adjacent to the corresponding functional element. Figure 13 shows the acceleration vibration level difference (VLD) of the measuring points in each metamaterial, and the VLDs of these measuring points reflect the vibration reduction performance of the corresponding adjacent functional element. Briefly, according to the definition of Eq. (3), the acceleration VLD of the points i and j can be expressed as

$$\mathrm{VLD}_{i-j} = 20\log_{10}\left(\frac{a_i}{a_j}\right) \tag{16}$$

where a_i and a_j represent the acceleration response of the measuring points i and j.

The data in Fig. 13 show that the vibration amplitude is effectively suppressed after the vibration propagated through the metamaterials, which indicates that the series of metamaterials have the characteristics of vibration reduction. In addition, for a metamaterials specimen with a certain PR, the VLD value between measuring points of the functional element is larger as the functional element is located closer to the fixed lower faceplate. This phenomenon is affected by the boundary effect theory, and the VLD value between the two points closer to the fixed constraint position is larger; thus, the values of VLD_{A-B}, VLD_{B-C}, VLD_{C-D} and VLD_{D-E} are gradually increasing.

In addition, the sum of the VLD values of VLD_{A-B}, VLD_{B-C}, VLD_{C-D} and VLD_{D-E} is equal to that of VLD_{A-E}, which indicates that the vibration reduction effect of metamaterials can be converted by the accumulation of several functional elements. This phenomenon also means that for a metamaterials with periodic functional element arrangement, the VLD of the metamaterials can be calculated by cumulatively calculating the VLD of each functional element.

Table 2 Vertical first-order natural frequency of metamaterials corresponding to various PRs

$v = -0.5$	$v = -1.0$	$v = -1.5$	$v = -2.0$
183.6 Hz	269.3 Hz	271.1 Hz	285.8 Hz

Effect of Poisson's ratio on vibration reduction performance

In order to intuitively express the influence of PR on the vibration reduction performance of the four metamaterials, the performances comparison is based on the premise of choosing the measuring points with similar positions. Figure 14 shows the vibration reduction of metamaterials at measurement points A–B, B–C, C–D and D–E, respectively. In the range of 10–155 Hz, the vibration reduction effects increase as the absolute values of the PR increase. When the frequency is greater than 215 Hz, the vibration reduction effects of other metamaterials decrease

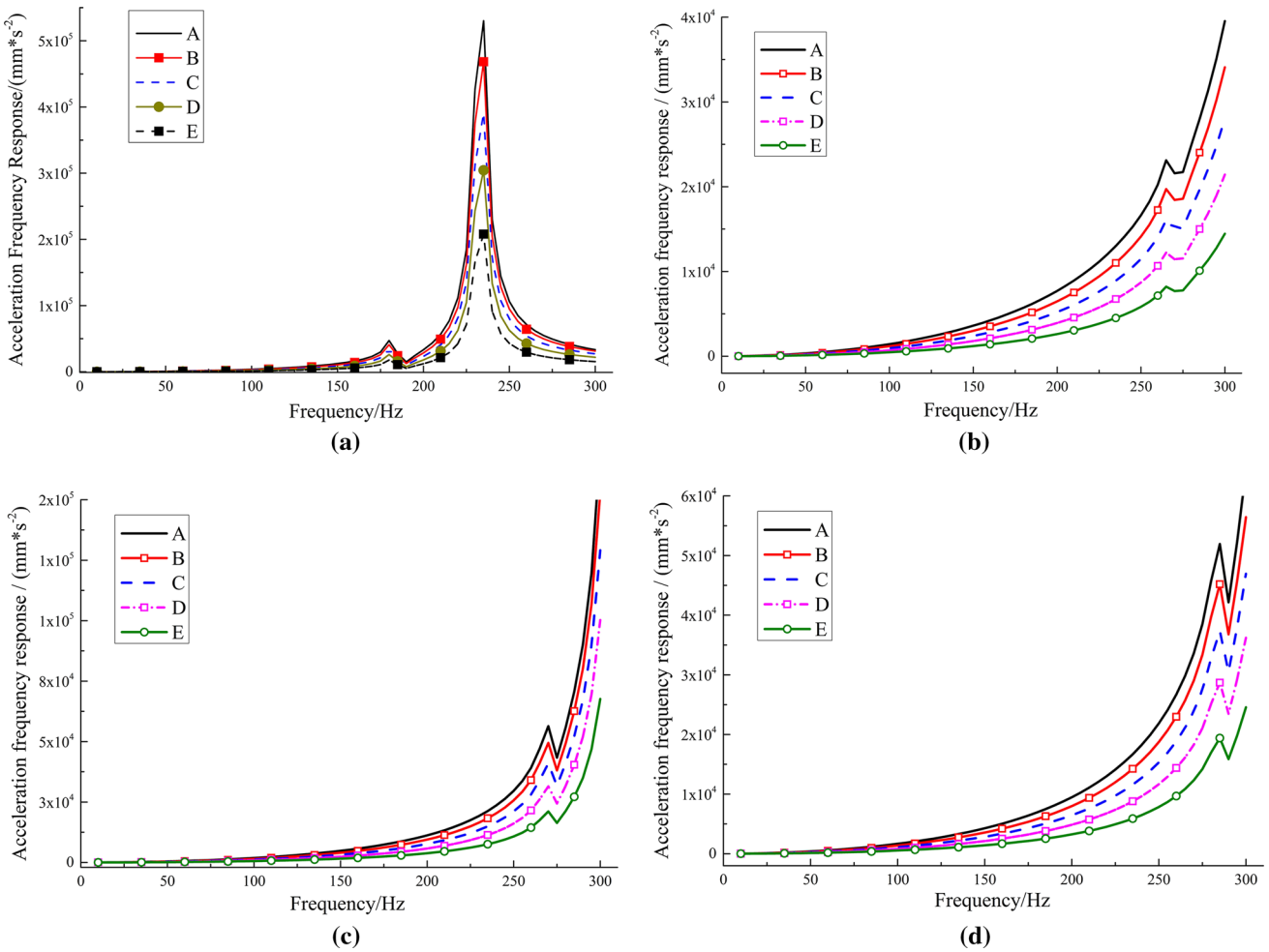

Figure 12 Frequency response of measuring points A, B, C, D and E corresponding to metamaterials structures with various PRs: **a** $v = -0.5$; **b** $v = -1.0$; **c** $v = -1.5$; and **d** $v = -2.0$.

with the increase in the absolute value of PR except for the metamaterials with $v = -0.5$.

However, more attention should be paid to the vibration reduction performance of the metamaterials structure in engineering applications, rather than the vibration reduction of the substructure (functional element) that makes up the metamaterials structures. Therefore, in this work, the vibration reduction performance of metamaterials is described by calculating the acceleration VLD between measuring points A–E, which is denoted by $\overline{\text{VLD}}$. Thus, the vibration reduction performance of the various novel designed metamaterials is summarized in Fig. 15.

Figure 15 shows the $\overline{\text{VLD}}$ curves of various metamaterials, and it can be seen that the $\overline{\text{VLD}}$ of the four metamaterials is greater than 7 dB in the frequency range of 10–300 Hz, which is equivalent to a 55.3% reduction after the vibration propagation through the metamaterials. In particular, the metamaterials with $v = -1.0$, $v = -1.5$ and $v = -2.0$ exhibit superior vibration reduction performance, and the $\overline{\text{VLD}}$ values range from 8.5 dB to 10 dB; thus, the amplitudes of the vibration are reduced by 62.4–68.4%. Consequently, the metamaterials designed with the goal of maximizing original impedance show excellent vibration reduction performance.

Evaluation of vibration reduction performance

The honeycomb materials in [46] is introduced as a comparison to illustrate the vibration reduction performance of the novel designed metamaterials. As shown in Fig. 16, the wall thickness and material's parameters of the honeycomb in [46] are consistent

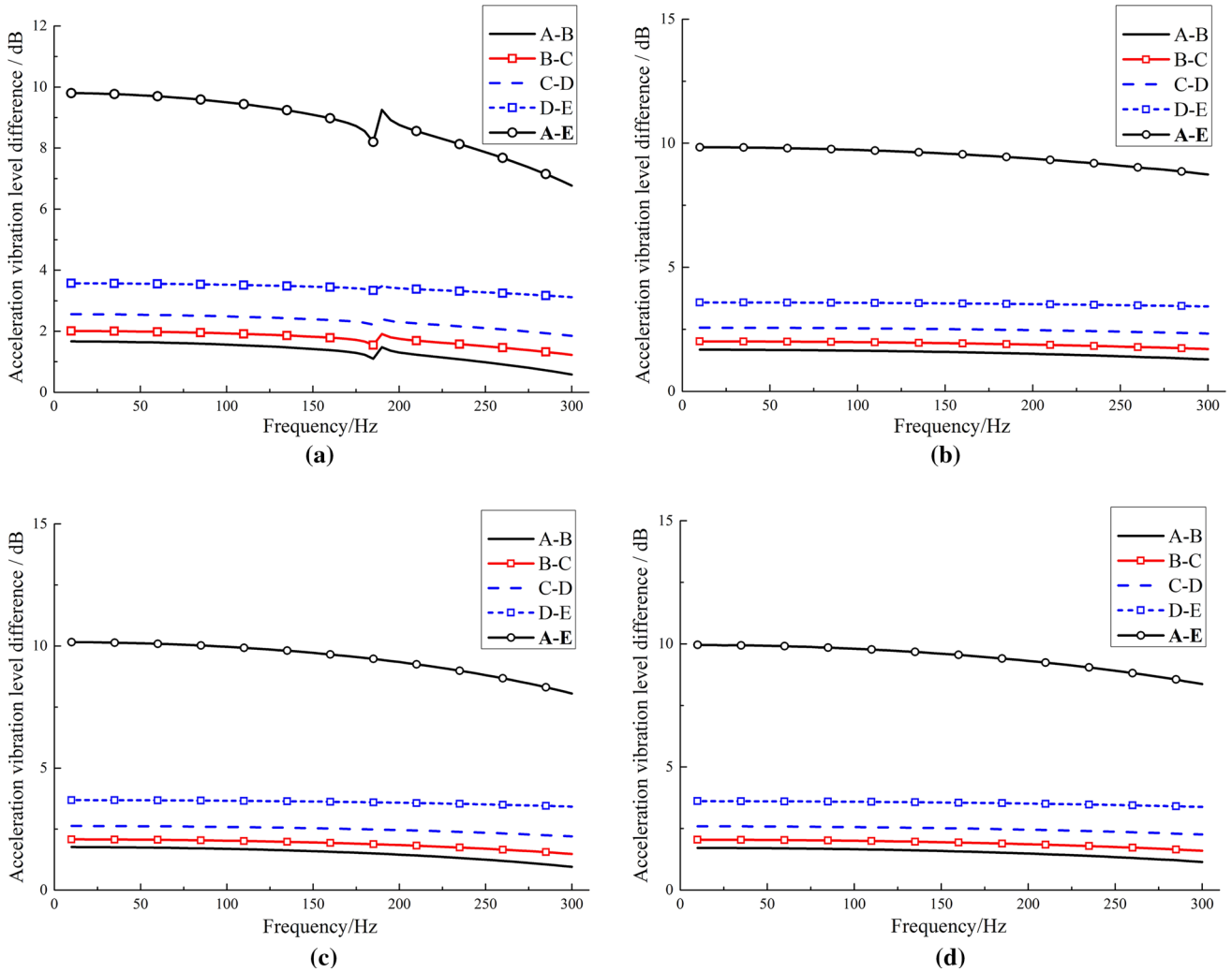

Figure 13 VLD between measuring points A–B, B–C, C–D, D–E and A–E corresponding to metamaterials with various PRs: **a** $v = -0.5$; **b** $v = -1.0$; **c** $v = -1.5$; and **d** $v = -2.0$.

with this work, and the loading and boundary conditions of the honeycomb are the same as in this work.

In this work, the two methods of vibration level difference (VLD) and frequency response are used to evaluate the vibration effect of metamaterials. The VLD measures the attenuation amplitude of the vibration wave between the two responses, so the VLD can easily reflect the relative change of the vibration amplitude between various responses in the same metamaterials. And the larger the value of VLD is, the greater the attenuation of the vibration wave between the two responses of measuring points, that is, the better the vibration reduction performance.

The frequency response analysis is able to effectively compare the response amplitude of the output of each metamaterial under the same excitation force. That is, the difference in vibration reduction performance between each of the metamaterials can be judged by comparing the amplitude of the responses at the respective output position, and the smaller the amplitude of the output response, the better the vibration reduction performance of the metamaterials.

Evaluation of vibration reduction performance with VLD

The data in Fig. 15 are further analyzed, and the curves of $\overline{\mathrm{VLD}}$ in the range of 10–300 Hz are converted as a synthesized value $\overline{\mathrm{VLD}}^{\mathrm{all}}$.

$$\overline{\mathrm{VLD}}^{\mathrm{all}} = \frac{1}{Q}\sum_{i=1}^{Q} \overline{\mathrm{VLD}}_{f_i} \tag{17}$$

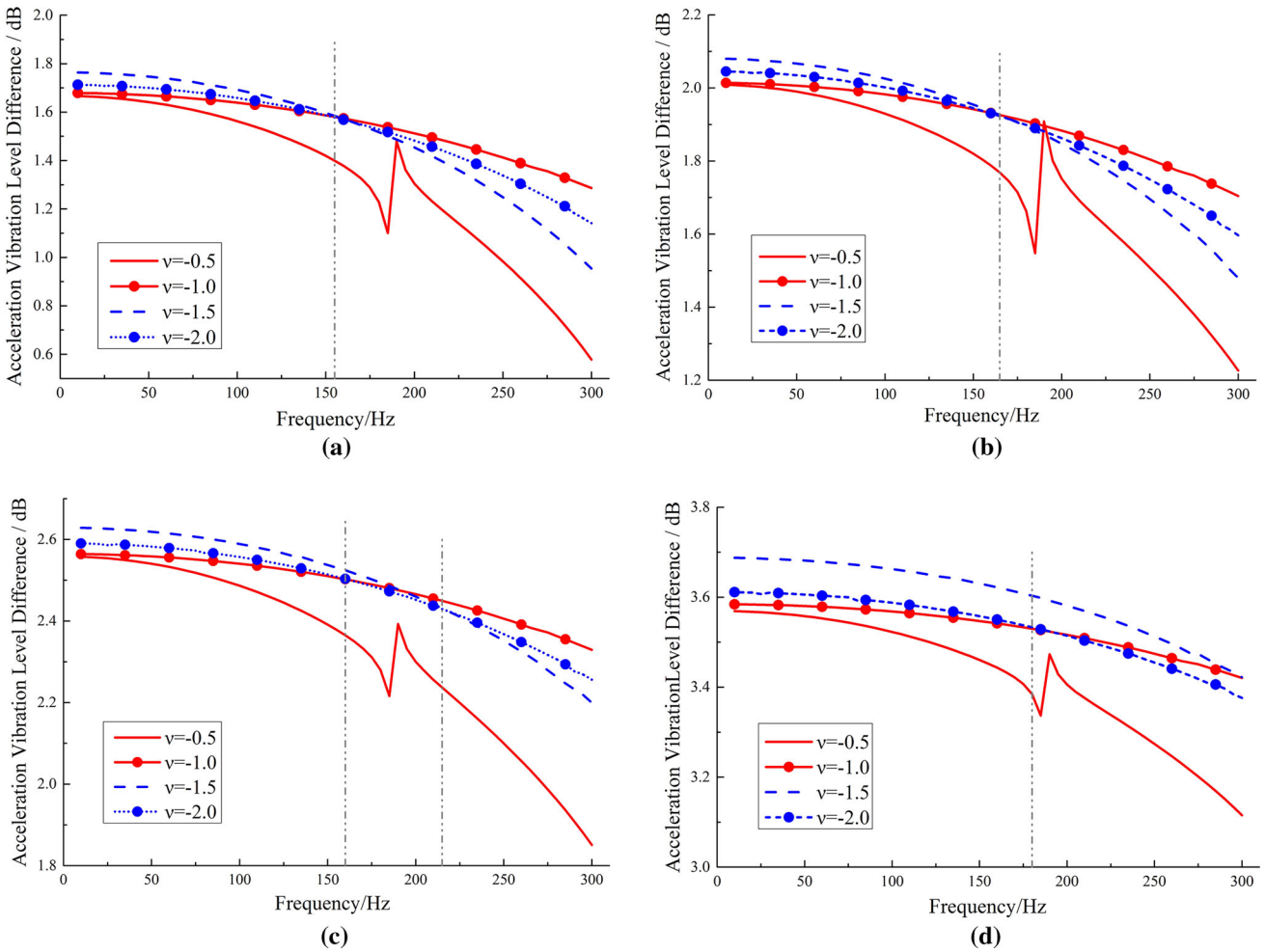

Figure 14 Vibration reduction effect of each PR metamaterials at measuring points: **a** A–B; **b** B–C; **c** C–D; and **d** D–E.

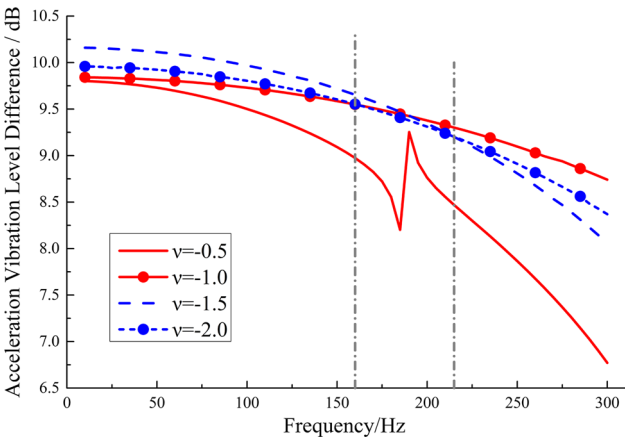

Figure 15 Vibration reduction performance $\overline{\text{VLD}}$ of various PR metamaterials.

where $f_i = 10 + 5i$ Hz, $i = 1, 2, \ldots, Q$, and $Q = 58$ when the sweep range is within 10–300 Hz. $\overline{\text{VLD}}_{f_i}$ represents the amplitude of $\overline{\text{VLD}}$ at the specified frequency f_i.

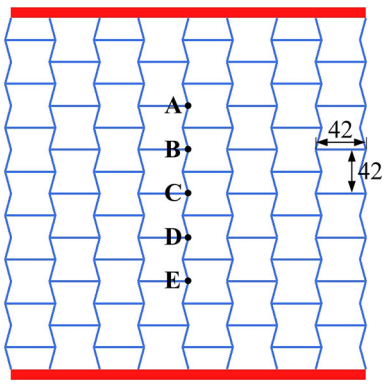

Figure 16 Honeycomb specimen with $v = -2.0$.

Figure 17 shows the acceleration VLD curves between the measuring points A and E of the honeycomb. Although the vibration reduction effect of

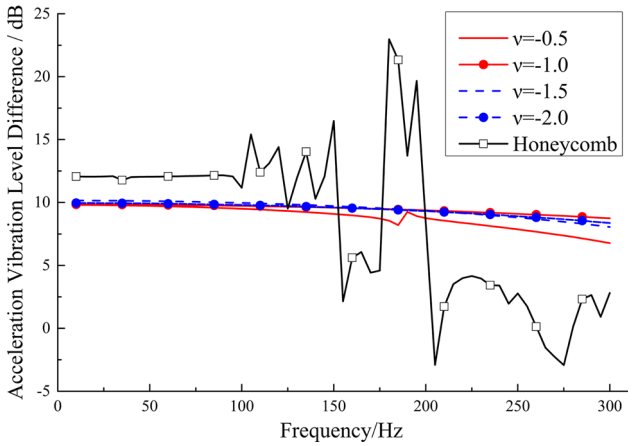

Figure 17 Acceleration vibration level difference of the novel designed metamaterials and honeycomb.

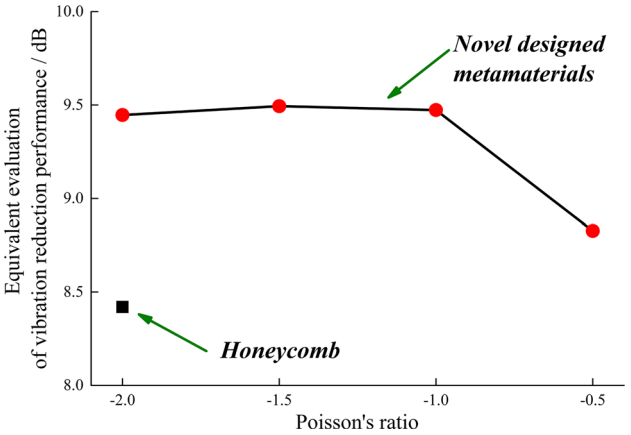

Figure 18 Vibration level difference of the novel designed metamaterials and honeycomb.

the honeycomb in the local frequency band is better, the vibration amplification begins to appear after the frequency is higher than 150 Hz, which is contrary to the intention of vibration reduction. Furthermore, the synthesized vibration reduction effect of the honeycomb is calculated by Eq. (17) as $\overline{\mathrm{VLD}}_{\mathrm{H}}^{\mathrm{all}} = 8.5$ dB. From Fig. 18, the performance of the novel metamaterials is 1 dB higher than that of the honeycomb. (The vibration reduction performance is improved by 12%.)

The synthesized vibration reduction effect $\overline{\mathrm{VLD}}^{\mathrm{all}}$ of the four metamaterials is shown in Fig. 18, and $\overline{\mathrm{VLD}}^{\mathrm{all}}$ are all greater than 8.5 dB; thus, the amplitude of the vibration is reduced by 62.4%. In particular, the vibration reduction performance of the metamaterials with $v = -1.0$, $v = -1.5$ and $v = -2.0$ is prominent. (The value of $\overline{\mathrm{VLD}}^{\mathrm{all}}$ is about 9.5 dB, and the vibration amplitude is reduced by 66.5%.)

In summary, the novel designed metamaterials exhibit better vibration reduction performance than the honeycomb, and the vibration reduction characteristics are stable and reliable.

Evaluation of vibration reduction performance with frequency response

In addition to using VLD to indicate the vibration propagation attenuation in materials or structures, the acceleration frequency responses at the measuring point E in novel metamaterials and honeycomb are analyzed simultaneously (as shown in Fig. 19), and the acceleration response of measuring point E is denoted by $\bar{a}$. An equivalent evaluation similar to the

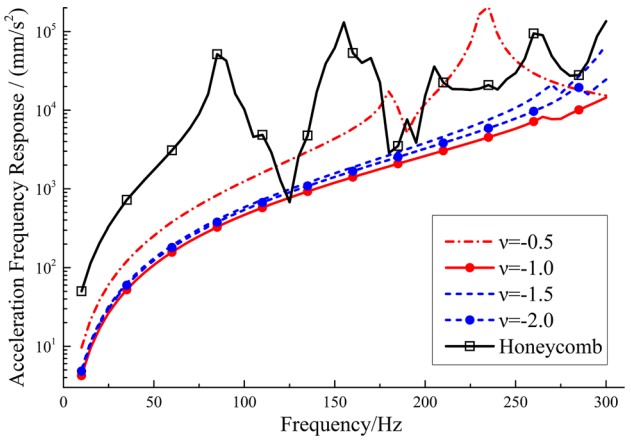

Figure 19 Acceleration frequency response of the novel designed metamaterials and honeycomb.

one defined in Eq. (17) is used to describe the value of the synthesized acceleration $\bar{a}^{\mathrm{all}}$ in the range of 10–300 Hz:

$$\bar{a}^{\mathrm{all}} = \frac{1}{Q}\sum_{i=1}^{Q} \bar{a}_{f_i} \tag{18}$$

where $f_i = 10 + 5i$ Hz, $i = 1, 2, \ldots, Q$, and $Q = 58$ when the sweep range is within 10–300 Hz. $\bar{a}_{f_i}$ represents the amplitude of $\bar{a}$ at the specified frequency f_i.

According to Eq. (18), the synthesized acceleration of the four metamaterials and honeycomb is represented by $\bar{a}_{-0.5}^{\mathrm{all}}$, $\bar{a}_{-1.0}^{\mathrm{all}}$, $\bar{a}_{-1.5}^{\mathrm{all}}$, $\bar{a}_{-2.0}^{\mathrm{all}}$ and $\bar{a}_{\mathrm{H}}^{\mathrm{all}}$, respectively. From Table 3, it is observed that the synthesized acceleration of the four metamaterials is lower than that of the honeycomb. In order to more intuitively compare the difference between the vibration

Table 3 Vibration reduction effects of metamaterials relative to honeycomb

Poisson's ratio	Honeycomb	$v = -0.5$	$v = -1.0$	$v = -1.5$	$v = -2.0$
Synthesized acceleration response $\bar{a}^{\text{all}}$ (mm/s^2)	$\bar{a}^{\text{all}}_{\text{H}} = 2.52 \times 10^4$	$\bar{a}^{\text{all}}_{-0.5} = 1.85 \times 10^4$	$\bar{a}^{\text{all}}_{-1.0} = 2.82 \times 10^3$	$\bar{a}^{\text{all}}_{-1.5} = 6.59 \times 10^3$	$\bar{a}^{\text{all}}_{-2.0} = 4.11 \times 10^3$
Vibration reduction performance (compared to honeycomb)/dB		2.7 dB	19.0 dB	11.7 dB	15.8 dB

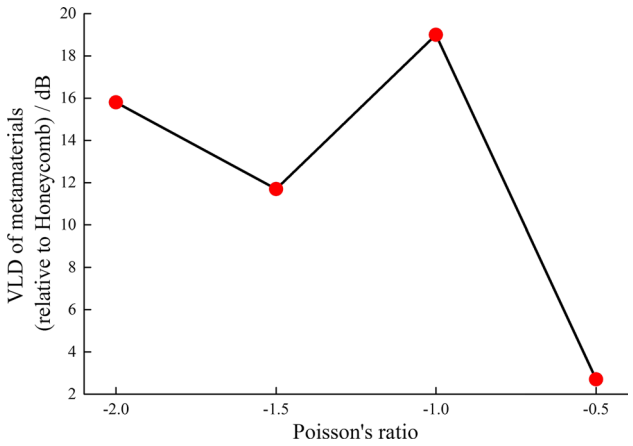

Figure 20 Vibration reduction effects of the metamaterials (relative to the honeycomb).

reduction effects of the four metamaterials and honeycomb, the vibration reduction effects of the four metamaterials relative to the honeycomb can be calculated by the following formula:

$$\text{VLD}_v = 20\log(\bar{a}^{\text{all}}_{\text{H}}/\bar{a}^{\text{all}}_{v}) \tag{19}$$

where $\bar{a}^{\text{all}}_{v}$ represents the synthesized acceleration of the metamaterials with $v = -0.5, -1.0, -1.5, -2.0$. As shown in Table 3 and Fig. 20, the vibration reduction of the four metamaterials relative to the honeycomb is calculated by Eq. (19).

By comparing the vibration reduction of the four metamaterials relative to the honeycomb, it shows that the vibration reduction performance of the novel designed metamaterials is obvious. In particular, the acceleration response of the metamaterials with $v = -1.0$ is reduced by 19 dB (in Fig. 20), which means that the magnitude of the acceleration response is reduced by 88.8%.

Conclusions

This work proposes a vibration reduction design method of metamaterials for improving the vibration reduction performance. The concrete conclusions are as follows:

(1) A FETO-based vibration reduction design method of metamaterials is proposed, and a series of negative PR metamaterials with novel configurations are designed. Numerical simulation shows that the error rate of the optimized PR and PR design requirements is less than 10%, which illustrated the feasibility of the proposed design method.

(2) Frequency response shows that the vibration amplitudes of the all designed metamaterials are reduced by 62.4%, and it is demonstrated that the metamaterials design with vibration reduction performance can be obtained by maximizing mechanical impedance as an optimization goal.

(3) Comparison shows that the novel designed metamaterials exhibit at least 12% improvement in vibration reduction performance over the honeycomb, and the vibration reduction performance is stable and reliable.

In addition to being the objective of the optimization, the specified vibration reduction performance can also be used as a constraint for the optimization problem. For example, the mathematical model of optimization can be established as follows: With a vibration reduction effect greater than 4 dB as a constraint, the mathematical model can be constructed with the goal of minimum total weight to design lightweight metamaterials.

Acknowledgements

This work was supported by the National Natural Science Foundation of China [Grant No. 51479115], High-tech Ship Research Projects by MIIT [Grant Nos. [2014]148, [2016]548] and Opening Project by the State Key Laboratory of Ocean Engineering [Grant No. GKZD010071].

Author Contributions

HQ and DY put forward the theoretical method of topology optimization of functional element; HQ calculated and analyzed the topology optimization model; HQ, DY analyzed the data; Deqing Yang contributed reagents/materials/analysis tools; and HQ wrote the paper.

Compliance with ethical standards

Conflicts of interest The authors declare no conflict of interest.

References

[1] Evans KE, Nkansah MA, Hutchinson IJ et al (1991) Molecular network design. Nature 353:124–125. https://doi.org/10.1038/353124a0

[2] Saxena KK, Das R, Calius EP (2016) Three decades of auxetics research—materials with negative Poisson's ratio: a review. Adv Eng Mater 18(11):1847–1870. https://doi.org/10.1002/adem.201600053

[3] Kolken HMA, Zadpoor AA (2017) Auxetic mechanical metamaterials. RSC Adv 7(9):5111–5129. https://doi.org/10.1039/C6RA27333E

[4] Robbins J, Owen SJ, Clark BW et al (2016) An efficient and scalable approach for generating topologically optimized cellular structures for additive manufacturing. Addit Manuf 12:296–304. https://doi.org/10.1016/j.addma.2016.06.013

[5] Yang W, Li ZM, Shi W et al (2004) Review on auxetic materials. J Mater Sci 39(10):3269–3279. https://doi.org/10.1023/B:JMSC.000

[6] Hu LL, Deng H (2015) Indentation resistance of the re-entrant hexagonal honeycombs with negative Poisson's ratio. Mater Res Innov 19(sup 1):S1-442–S1-445. https://doi.org/10.1179/1432891715Z.0000000001588

[7] Compton BG, Lewis JA (2014) 3D-printing of lightweight cellular composites. Adv Mater 26(34):5930–5935. https://doi.org/10.1002/adma.201401804

[8] Nia AA, Razavi SB, Majzoobi GH (2008) Ballistic limit determination of aluminum honeycombs-experimental study. Mater Sci Eng A 488(1–2):273–280. https://doi.org/10.1016/j.msea.2007.11.044

[9] Yungwirth CJ, Wadley HNG, O'Connor JH et al (2008) Impact response of sandwich plates with a pyramidal lattice core. Int J Impact Eng 35(8):920–936. https://doi.org/10.1016/j.ijimpeng.2007.07.001

[10] Fleck NA, Deshpande VS, Ashby MF (2010) Micro-architectured materials: past, present and future. Proc Mathem Phys Eng Sci 466(2121):2495–2516. https://doi.org/10.1098/rspa.2010.0215

[11] Li Dong, Yin Jianhua, Dong Liang et al (2018) Strong re-entrant cellular structures with negative Poisson's ratio. J Mater Sci 53:3493–3499. https://doi.org/10.1007/s10853-017-1809-8

[12] Chekkal I, Remillat C, Scarpa F (2003) Acoustic properties of auxetic foams. High Perform Struct Mater 6:119–129. https://doi.org/10.2495/HPSM120111

[13] Boldrin L, Hummel S, Scarpa F et al (2016) Dynamic behaviour of auxetic gradient composite hexagonal honeycombs. Compos Struct 149:114–124. https://doi.org/10.1016/j.compstruct.2016.03.044

[14] Scarpa F, Tomlinson G (2000) Theoretical characteristics of the vibration of sandwich plates with in-plane negative Poisson's ratio values. J Sound Vib 230(1):45–67. https://doi.org/10.1006/jsvi.1999.2600

[15] Nguyen DD, Pham CH (2016) Nonlinear dynamic response and vibration of sandwich composite plates with negative Poisson's ratio in auxetic honeycombs. J Sandwich Struct Mater 20:692–717. https://doi.org/10.1177/1099636216674729

[16] Duc ND, Kim SE, Cong PH, Anh NT, Khoa ND (2017) Dynamic response and vibration of composite double curved shallow shells with negative Poisson's ratio in auxetic honeycombs core layer on elastic foundations subjected to blast and damping loads. Int J Mech Sci 133:504–512. https://doi.org/10.1016/j.ijmecsci.2017.09.009

[17] Duc ND, Cong PH (2018) Nonlinear dynamic response and vibration of sandwich composite plates with negative Poisson's ratio in auxetic honeycombs. J Sandwich Struct Mater 20(6):692–717. https://doi.org/10.1177/1099636216674729

[18] Yang W, Li ZM, Shi W et al (2004) Review on auxetic materials. J Mater Sci 39(10):3269–3279. https://doi.org/10.1023/B:JMSC.0000026928.93231.e0

[19] Bianchi M, Scarpa F (2013) Vibration transmissibility and damping behaviour for auxetic and conventional foams under linear and nonlinear regimes. Smart Mater Struct 22(8):084010. https://doi.org/10.1088/0964-1726/22/8/084010

[20] Scarpa FL, Bullough WA, Lumley P (2004) Trends in acoustic properties of iron particle seeded auxetic polyurethane foam. ARCHIVE Proc Inst Mech Eng Part C J Mech Eng Sci 203–210(2):241. https://doi.org/10.5150/jngcgc.2004.057-S

[21] Chekkal I, Bianchi M, Remillat C et al (2010) Vibro-Acoustic properties of auxetic open cell foam: model and experimental results. Acta Acustica United Acustica 96(2):266–274. https://doi.org/10.3813/AAA.918276

[22] Duc ND, Bich DH, Cong PH (2016) Nonlinear thermal dynamic response of shear deformable FGM plates on elastic foundations. J Therm Stresses 39(3):278–297. https://doi.org/10.1080/01495739.2015.1125194

[23] Duc ND, Quan TQ, Khoa ND (2017) New approach to investigate nonlinear dynamic response and vibration of imperfect functionally graded carbon nanotube reinforced composite double curved shallow shells. Aerosp Sci Technol 71:360–372. https://doi.org/10.1016/j.ast.2017.09.031

[24] Ajdari A, Babaee S, Vaziri A (2011) Mechanical properties and energy absorption of heterogeneous and functionally graded cellular structures. Proc Eng 1:219–223. https://doi.org/10.1016/j.proeng.2011.04.039

[25] Prawoto Y (2012) Seeing auxetic materials from the mechanics point of view: a structural review on the negative Poisson's ratio. Comput Mater Sci 58:140–153. https://doi.org/10.1016/j.commatsci.2012.02.012

[26] Liebold-Ribeiro Yvonne, Körner Carolin (2014) Phononic band gaps in periodic cellular materials. Adv Eng Mater 16(3):328–334. https://doi.org/10.1002/adem.201300064

[27] Catapano A, Montemurro M (2014) A multi-scale approach for the optimum design of sandwich plates with honeycomb core. Part II: the optimisation strategy. Compos Struct 118:677–690. https://doi.org/10.1016/j.compstruct.2014.07.057

[28] Seepersad CC, Kumar RS, Allen JK et al (2004) Multi-functional design of prismatic cellular materials. J Comput Aided Mater Des 11(2–3):163–181. https://doi.org/10.1007/s10820-005-3167-0

[29] Seepersad CC, Allen JK, Mcdowell DL et al (2008) Multi-functional topology design of cellular material structures. J Mech Des 130(3):031404. https://doi.org/10.1115/1.2829876

[30] Ju J, Summers JD, Ziegert J, et al (2009) Design of honeycomb meta-materials for high shear flexure. In: ASME 2009 international design engineering technical conferences and computers and information in engineering conference. American Society of Mechanical Engineers, pp 805–813. https://doi.org/10.1115/DETC2009-87730

[31] Boucher MA, Smith CW, Scarpa F et al (2013) Effective topologies for vibration damping inserts in honeycomb structures. Compos Struct 106:1–14. https://doi.org/10.1016/j.compstruct.2013.05.036

[32] Strek T, Jopek H, Idczak E (2016) Computational design of two-phase auxetic structures. Physica status solidi (b) 253(7):1387–1394. https://doi.org/10.1002/pssb.201600120

[33] Radman A, Huang X, Xie YM (2013) Topology optimization of functionally graded cellular materials. J Mater Sci 48(4):1503–1510. https://doi.org/10.1007/s10853-012-6905-1

[34] Findeisen C, Hohe J, Kadic M, Gumbsch P (2017) Characteristics of mechanical metamaterials based on buckling elements. J Mech Phys Solids 102:151–164. https://doi.org/10.1016/j.jmps.2017.02.011

[35] Xu B, Huang X, Xie YM (2016) Two-scale dynamic optimal design of composite structures in the time domain using equivalent static loads. Compos Struct 142:335–345. https://doi.org/10.1016/j.compstruct.2016.01.090

[36] Long K, Han D, Gu X (2017) Concurrent topology optimization of composite macrostructure and microstructure constructed by constituent phases of distinct Poisson's ratios for maximum frequency. Comput Mater Sci 129:194–201. https://doi.org/10.1016/j.commatsci.2016.12.013

[37] Qin H, Yang D, Ren C (2018) Modelling theory of functional element design for metamaterials with arbitrary negative Poisson's ratio. Comput Mater Sci 150:121–133. https://doi.org/10.1016/j.commatsci.2018.03.056

[38] Pradhan PK, Mandal A, Baidya DK et al (2008) Dynamic response of machine foundation on layered soil: cone model versus experiments. Geotech Geol Eng 26(4):453–468. https://doi.org/10.1007/s10706-008-9181-8

[39] Qi Libo, Zou Mingsong, Liu Shuxiao et al (2019) Use of impedance mismatch in the control of coupled acoustic radiation of the submarine induced by propeller-shaft system. Mar Struct 65:249–258. https://doi.org/10.1016/j.marstruc.2019.02.001

[40] Grima JN, Manicaro E, Attard D (2011) Auxetic behaviour from connected different-sized squares and rectangles. Proc R Soc Lon A: Math Phys Eng Sci R Soc 467(2126):439–458. https://doi.org/10.1098/rspa.2010.0171

[41] Gibson LJ, Ashby MF (1999) Cellular solids: structure and properties. Cambridge University Press, Cambridge

[42] Grima JN, Gatt R, Ellul B et al (2010) Auxetic behaviour in non-crystalline materials having star or triangular shaped perforations. J Non-Cryst Solids 356(37–40):1980–1987. https://doi.org/10.1016/j.jnoncrysol.2010.05.074

[43] Schwerdtfeger J, Wein F, Leugering G et al (2011) Design of auxetic structures via mathematical optimization. Adv Mater 23(22–23):2650–2654. https://doi.org/10.1002/adma.201004090

[44] Guoyang Guan, Guiqiong Jiao, Zengguang Zhang (2005) Uniaxial macro-mechanical property and failure mode of a

2D-moven C/SiC composite. Acta Materiae Compositae Sinica 22(4):81–85. https://doi.org/10.3321/j.issn:1000-3851.2005.04.014

[45] Carneiro VH, Puga H, Meireles J (2016) Analysis of the geometrical dependence of auxetic behavior in reentrant structures by finite elements. Acta Mech Sin 32(2):295–300. https://doi.org/10.1007/s10409-015-0534-2

[46] Zhang XW, Yang DQ (2016) Mechanical properties of auxetic cellular material consisting of re-entrant hexagonal honeycombs. Materials 9(11):900. https://doi.org/10.3390/ma9110900

[47] Hönig A, Stronge WJ (2002) In-plane dynamic crushing of honeycomb. Part I: crush band initiation and wave trapping. Int J Mech Sci 44(8):1665–1696. https://doi.org/10.1016/S0020-7403(02)00060-7